Agricultural and Forest Meteorology 331 (2023) 109350

Contents lists available at ScienceDirect

Agricultural and Forest Meteorology

journal homepage: www.elsevier.com/locate/agrformet

Asymmetric response of primary productivity to precipitation anomalies in Southwest China

Guanyu Dong [a,b], Lei Fan [a,b,*], Rasmus Fensholt [c], Frédéric Frappart [d,j], Philippe Ciais [e], Xiangming Xiao [f], Stephen Sitch [g], Zanpin Xing [h], Ling Yu [a,b], Zhilan Zhou [a,b], Mingguo Ma [a,b], Xiaowei Tong [c], Qing Xiao [i], Jean-Pierre Wigneron [d,j]

[a] Chongqing Jinfo Mountain Karst Ecosystem National Observation and Research Station, School of Geographical Sciences, Southwest University, Chongqing 400715, China
[b] Chongqing Engineering Research Center for Remote Sensing Big Data Application, School of Geographical Sciences, Southwest University, Chongqing 400715, China
[c] Department of Geosciences and Natural Resource Management, University of Copenhagen, Copenhagen, Denmark
[d] INRAE, Bordeaux Sciences Agro, UMR 1391 ISPA, 33140 Villenave-d'Ornon, France
[e] Laboratoire des Sciences du Climat et de l'Environnement, LSCE/IPSL, CEA-CNRS-UVSQ, Université Paris-Saclay, 91191 Gif-Sur-Yvette, France
[f] Department of Microbiology and Plant Biology, Center for Earth Observation and Modeling, University of Oklahoma, Norman, OK 73019, USA
[g] College of Life and Environmental Sciences, University of Exeter, Exeter EX4 4RJ, UK
[h] Cryosphere Research Station on the Qinghai-Tibet Plateau, State Key Laboratory of Cryospheric Science, Northwest Institute of Eco-Environment and Resource, Chinese Academy of Sciences, Lanzhou, Gansu 730000, China
[i] State Key Laboratory of Remote Sensing Science, Aerospace Information Research Institute, Chinese Academy of Sciences, Beijing 100101, China
[j] Université de Bordeaux, 33400 Talence, France

ARTICLE INFO

Keywords:
Asymmetric response
Vegetation primary productivity
Precipitation anomalies
Southwest China

ABSTRACT

Southwest China has been the largest terrestrial carbon sink in China over the past 30 years, but has recently experienced a succession of droughts caused by high precipitation variability, potentially threatening vegetation productivity in the region. Yet, the impact of precipitation anomalies on the vegetation primary productivity is poorly known. We used an asymmetry index (AI) to explore possible asymmetric productivity responses to precipitation anomalies in Southwest China from 2003 to 2018, using a precipitation dataset, combined with gross primary productivity (GPP), net primary productivity (NPP), and vegetation optical depth (VOD) products. Our results indicate that the vegetation primary productivity of Southwest China shows a negative asymmetry, suggesting that the increase of vegetation primary productivity during wet years exceeds the decrease during dry years. However, this negative asymmetry of vegetation primary productivity was shifted towards a positive asymmetry during the period of analysis, suggesting that the resistance of vegetation to drought, has increased with the rise in the occurrence of drought events. Among the different biomes, grassland vegetation primary productivity had the highest sensitivity to precipitation anomalies, indicating that grasslands are more flexible than other biomes and able to adjust primary productivity in response to precipitation anomalies. Furthermore, our results showed that the asymmetry of vegetation primary productivity was influenced by the effects of temperature, precipitation, solar radiation, and anthropogenic and topographic factors. These findings improve our understanding of the response of vegetation primary productivity to climate change over Southwest China.

1. Introduction

Southwest China, mainly covered by subtropical vegetation, represents one of the largest terrestrial carbon sinks in China over the past 30 years (Liu et al., 2016; Piao et al., 2009). However, this carbon sink and growth of vegetation are generally vulnerable to drought (Frank et al., 2015; Ge et al., 2021). Southwest China is the largest karst region in the world (Song et al., 2019), where the vegetation in this region is vulnerable to the seasonal drought (Liu et al., 2012). Also, the relatively low soil moisture cannot meet the demand of land surface evapotranspiration due to the low water-holding capacity (Liu et al., 2011a), leading to widespread water stress on vegetation.

* Corresponding author.
E-mail address: leifan33@swu.edu.cn (L. Fan).

https://doi.org/10.1016/j.agrformet.2023.109350
Received 24 November 2022; Received in revised form 18 January 2023; Accepted 27 January 2023
Available online 2 February 2023

In recent years, large-scale afforestation and intensive ecological restoration projects have been implemented to alleviate land degradation (Yue et al., 2022), making Southwest China a hotspot region for the increase in vegetation cover and aboveground biomass (Brandt et al., 2018). Simultaneously, a recent study reported that vegetation in Southwest China still has strong carbon sink potential (Zhang et al., 2022), and optimizing current forestation projects could generate a long-term and sustainable carbon sink in the future. Yet, extreme drought events occurred frequently, leading to a large decrease in vegetation productivity during the drought period (Tong et al., 2018). Thus, it is essential to understand the response of carbon dynamics to climate changes over Southwest China.

Previous studies have already analyzed the intensity and frequency of extreme drought events in Southwest China, as well as the vegetation response and the legacy effects of drought. For instance, multiple drought metrics showed that the frequency and duration of drought events in this region have increased from 2000 to 2014, concurrent with rising temperature and decreasing precipitation (Li et al., 2014; Zhang et al., 2013). Also, extreme drought events could suppress vegetation growth, reducing vegetation productivity and its carbon sequestration capacity (Zhang et al., 2012). Furthermore, vegetation in this region has capacity to recover its greenness and productivity from the effects of drought within 6 months, primarily due to subsequent increased precipitation, climate warming, and land management (Chen et al., 2021; Li et al., 2019).

However, few studies investigated the asymmetry of vegetation primary productivity in response to precipitation anomalies over Southwest China, that is, the comparison between the increase in vegetation primary productivity during wet years and the decrease in vegetation primary productivity during dry years. Improving this knowledge is crucial for a better understanding of carbon budget and resilience of terrestrial ecosystems.

Current studies about the asymmetry of vegetation productivity in response to precipitation anomalies were mainly made over arid and semi-arid areas (e.g., Africa, USA, and Australia), where vegetation productivity was highly sensitive to variations in water availability (Dannenberg et al., 2019). However, the magnitude of this asymmetric response could decrease with increasing mean annual precipitation (Al-Yaari et al., 2020), which posed challenges for monitoring the asymmetry of vegetation productivity in humid areas. Thus, only a few studies focused on humid areas (e.g., Southwest China). According to field studies, the primary productivity in arid grasslands, for instance, was more responsive to a wetter condition (Wilcox et al., 2017). Similar result could be found in the semi-arid regions (e.g., Australia, USA), in which a positive asymmetry in vegetation productivity were observed (Haverd et al., 2017). Higher interannual rainfall variability was reported to favor a more dynamic vegetation response to rainfall anomalies when comparing different semi-arid ecosystems in West Africa using remote sensing data (Ratzmann et al., 2016).

A comprehensive assessment of the asymmetric response of vegetation productivity to precipitation anomalies in the humid region is necessary for a better understanding of the ecosystem function under climate change. Southwest China is a humid region with a subtropical monsoon climate, different from previous studies in terms of rainfall and climate. Recently, extreme climate events over Southwest China have occurred frequently, with the most severe and sustained drought events occurring in the summer of 2006, 2009/2010 winter-spring, and the summer periods of 2011 and 2013 (Li et al., 2011; Long et al., 2014; Yuan et al., 2016). These extreme drought events provide an ideal foundation for studying the asymmetry of vegetation primary productivity in response to precipitation anomalies in humid regions.

Here, multiple satellite-observed and model simulation data (gross primary productivity (GPP), net primary productivity (NPP), vegetation optical depth (VOD), precipitation) and two different asymmetric index quantification methods (see Methods) were used to assess the asymmetry of vegetation productivity in response to precipitation anomalies over Southwest China from 2003 to 2018. The goals of this study are: (1) to investigate the asymmetric response of primary productivity to extreme drought events and its general trend during the recent two decades over Southwest China, and (2) to analyze the main environmental factors associated with the asymmetric response.

2. Materials and methods

2.1. Study area

The Southwest China (96°21′-112°04′E; 20°54′-34°19′N), covering an area of 1.37×106 km^2, includes Sichuan, Yunnan, Guizhou, and Guangxi Provinces, as well as the Chongqing municipality (Fig. 1). Southwest China, characterized by a subtropical monsoon climate, has a distinctive karst landscape and its elevation progressively rises from the southeast to the northwest (Wang et al., 2021). Furthermore, vegetation is highly fragile owing to the impact of geology, landforms, climate, and human activity (Wang et al., 2010). For example, karst regions are vulnerable to the change of environment and human activities, resulting in severe soil erosion and rocky desertification. In addition, the growing population over the past three decades has increased the demand for water and natural resources (Hao et al., 2015).

In this study, the International Geosphere Programme (IGBP) scheme of land cover classification was used as the basis for the creation of land cover types (Loveland and Belward, 1997). It contains 17 types of land cover. We selected the MODIS MCD12Q1 Land cover map at 500-m spatial resolution from 2001–2010 to get information about the land cover in Southwest China. Furthermore, we masked pixels of non-vegetation types, including “Urban and Built-Up”, “Snow and Ice”, “Water bodies”, and “Barren or sparse vegetated”, and aggregated to 25 km spatial resolution. Also, pixels which contained the “Wetland” land cover type were masked, because VOD is underestimated when the observation footprint contains substantial open water bodies (Liu et al., 2011b). We combined evergreen needleleaf forest, evergreen broadleaf forest, deciduous needleleaf forest, deciduous broadleaf forest, and mixed forest into a forest. We further combined closed shrublands, open shrublands, woody savannas, and savannas into shrublands, and croplands and cropland/natural vegetation mosaic into croplands. Accordingly, the vegetation of Southwest China is stratified into four land cover classes: forest (39.24%), croplands (22.38%), shrublands (20.29%), and grasslands (18.09%), corresponding to different climate regimes.

2.2. Satellite and auxiliary datasets

Vegetation productivity products (GPP, NPP, VOD), climatic variables (precipitation, potential evapotranspiration, and land surface temperature), and auxiliary data (land cover, maximum rooting depth, DEM) were used in the present study. The GPP, NPP, and VOD were used to evaluate vegetation productivity in relation to the change of biomass and to calculate the asymmetry index (AI). This study focused on the period of 2003–2018, due to data limitations (VODCA C-VOD was available from June 2002 to 2018) and severe drought frequently occurring since the 2000s (Zhang et al., 2013). More details about the datasets were introduced below and summarized in Table 1.

2.2.1. Proxies of vegetation productivity

2.2.1.1. NPP dataset from the mod17a3hgf. The MODIS MOD17A3HGF V6 product provides a yearly NPP at 500-m spatial resolution, which is accumulated using whole 8-day available MOD15A2H product for each pixel (Running et al., 2019). All good-quality observations (according to the per-pixel associated QA flags) of NPP during 2003–2018 were used in this study.

2.2.1.2. GPP dataset from the vegetation photosynthesis model (VPM).

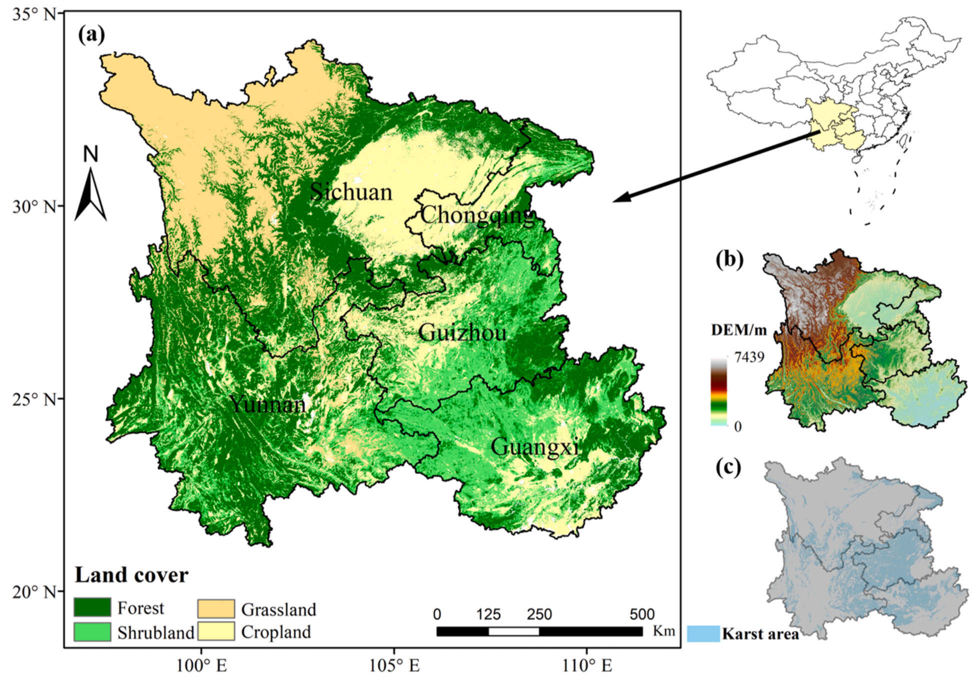

Fig. 1. The geographic location of Southwest China. (a) Land cover map of Southwest China based on 10 years (2001–2010) of MODIS MCD12Q1 data, (b) topographic map from the SRTM V3 DEM product, and (c) distribution of karst landscape from V3 world karst map.

Table 1
Overview of all data used in the present study.

Variables	Source	Spatial resolution	Temporal resolution	Time period	Reference
NPP	MOD17A3HGF	500m	yearly	2003–2018	(Running et al., 2019)
GPP	VPM	0.05°	yearly	2003–2018	(Zhang et al., 2021)
C-VOD	VODCA	0.25°	daily	2003–2018	(Moesinger et al., 2020)
NEE	ChinaFLUX		yearly	2003–2010	(Yu et al., 2006)
Precipitation	TerraClimate	4km	monthly	2003–2018	(Abatzoglou et al., 2018)
PET	TerraClimate	4km	monthly	2003–2018	(Abatzoglou et al., 2018)
LST	MOD11A1	1km	daily	2003–2018	(Wan et al., 2015)
Elevation	SRTM V3	30m			(Farr et al., 2007)
Max rooting depth		1km			(Fan et al., 2017)

The VPM GPP dataset (Zhang et al., 2021) is based on a satellite-based LUE model driven by satellite data from MODIS MOD09A1 surface reflectance, MCD12Q1 land cover, and MYD11A2 land surface temperature, as well as climate data from National Centers for Environmental Prediction (NCEP) reanalysis II. This dataset is available to the public and has three temporal resolutions (8-day, monthly, and annual) and three spatial resolutions (500-m, 0.05°, and 0.5°). A previous study shows that the VPM GPP could accurately represent the impacts on grasslands in drought years (Pei et al., 2020). Here, annual VPM GPP at 0.05° spatial resolution was selected.

2.2.1.3. Global long-term microwave vegetation optical depth climate archive (VODCA). Satellite-based VOD is widely used to monitor the dynamics of aboveground biomass (AGB) (Liu et al., 2015) and the impacts of drought events on vegetation over Southwest China (Brandt et al., 2018). A previous study (Moesinger et al., 2020) indicated that VODCA product exhibits high potential for detecting the change of ecosystem dynamics because of its sensitivity to water content of vegetation (VWC). Furthermore, VODCA, as long-term daily VOD products using the Land Parameter Retrieval Model (LPRM), includes three different spectral bands at the spatial resolution of 0.25°: C-band (2002–2018), X-band (1997–2018), and Ku-band (1987–2017). C-band VOD as the low-medium frequency band in VODCA products was used here, which can be accessed at https://zenodo.org/record/2575599.

Although VOD products based on L-band sensors (Konings et al., 2021) with a lower frequency and deeper penetration depths show higher sensitivity to VWC and AGB, the period covered by L-band VOD products starts in 2010, and, hence, cannot be used in the present study to analyze the long-term vegetation response.

2.2.1.4. Net ecosystem exchange (NEE) from in-situ observation. In this study, we obtained in-situ observational NEE data from the Xishuangbanna (XSBN) flux tower of the Chinese Terrestrial Ecosystem Flux Observation and Research Network (ChinaFLUX) (Yu et al., 2016). The XSBN site (101°1555"E, 21°5539"N) was in protected natural forests on the subtropical zone in Southwest China, providing yearly NEE data from 2003–2010 (Yu et al., 2006). This in-situ NEE data provides a unique opportunity to validate the interannual variation in the asymmetry of NPP, although NEE is a function of the difference between NPP and heterotrophic respiration (Rh).

2.2.2. Climatic variables

2.2.2.1. Precipitation and potential evapotranspiration (PET). TerraClimate, as a high-resolution global dataset, provides monthly climate data at 1/24° (~4 km) spatial resolution. It uses climatically aided interpolation, combining the WorldClim version 1.4 and version 2 datasets with CRU Ts4.0 and JRA-55 (Abatzoglou et al., 2018). Compared to gridded datasets with a coarser resolution, the TerraClimate dataset represented a considerable reduction in overall mean error and an increase in spatial realism (Abatzoglou et al., 2018). The precipitation and potential evapotranspiration (PET) data were selected in this study.

2.2.2.2. Land surface temperature (LST) dataset from the MOD11A1. The MODIS MOD11A1 V6 product provides a daily LST at a spatial resolution of 1 km (Wan et al., 2015). All good-quality observations (according to the per-pixel associated QA flags) of daytime LST were used as the source of the temperature data to investigate the drivers of asymmetry of vegetation productivity in response to precipitation anomalies.

2.2.3. Other auxiliary data

2.2.3.1. Maximum rooting depth. Plant rooting depth could affect the long-term carbon cycle and ecosystem resilience to drought (Fan et al., 2017). It was estimated at 30" (~1 km) global grids based on an inverse model driven by observed productivity and atmosphere (Fan et al., 2017). Therefore, the maximum rooting depth of root uptake averaged over 10 years (2004–2013) was selected to analyze the response of vegetation to precipitation change.

2.2.3.2. Elevation dataset from the shuttle radar topography mission (SRTM). Elevation has a significant effect on the frequency of extreme droughts (Zhang et al., 2013). Meanwhile, vegetation growth and its type are determined by the combination of various topographic factors (Laamrani et al., 2014). The SRTM V3 product provided by NASA JPL at a 30-m spatial resolution (Farr et al., 2007) was used as the source of the elevation data to investigate the drivers of asymmetry of vegetation productivity in response to precipitation anomalies.

In these datasets above, NPP, GPP, VOD, precipitation, PET, and LST were regridded to yearly values at a spatial resolution of 0.25° using a simple average method. Max rooting depth, land cover, and DEM were also regridded to a spatial resolution of 0.25°. Data pre-processing were processed on Google Earth Engine platform.

2.3. Methods

2.3.1. Asymmetry index (AI)

AI was used to measure the asymmetry of vegetation productivity in response to precipitation anomalies. In the present study, two methods were used for the calculation of the AI as proposed by Al-Yaari et al. (2020) based on wet and dry years (refer to Section 2.3.1.1) and (2) Haverd et al. (2017) based on extreme climate (refer to Section 2.3.1.2), as follows:

2.3.1.1. Asymmetry index calculated based on wet and dry years. According to Al-Yaari et al. (2020), AI can be defined as the difference between the increase of vegetation productivity during wet years and the decrease during dry years. Here, AI is calculated as follows (Al-Yaari et al., 2020):

$$Positive\ pulse = \frac{\max(Var) - mean(Var)}{abs(mean(Var))} \tag{1}$$

$$Negative\ decline = \frac{mean(Var) - \min(Var)}{abs(mean(Var))} \tag{2}$$

$$AI = Positive\ pulse - Negative\ decline \tag{3}$$

where var is the value of GPP, NPP, and VOD. *max* and *min* represent the highest and lowest values over the study period (2003–2018). *abs* and *mean* represent the absolute and mean yearly values. A *Positive pulse* and *Negative decline* represent the gain of variables during wet years and the decline of variables during dry years, respectively.

Furthermore, *AI* is calculated by the difference between *Positive pulse* and *Negative decline*. $AI > 0$ indicates a positive asymmetry, meaning that the increase of variables during wet years exceeds the decrease during dry years, and $AI < 0$ indicates a negative asymmetry, meaning that the decrease of variables during dry years exceeds the increase during wet years.

2.3.1.2. Asymmetry index calculated based on extreme climate. According to Haverd et al. (2016), the asymmetry index can also be defined by the difference between the change of vegetation productivity driven by precipitation extremes, and calculated by the outer pth percentiles of variables over the study period. Therefore, AI_p is calculated as follows (Haverd et al., 2016):

$$Positive\ pulse_p = \frac{mean(Var) - mean\left(Var_{+p}\right)}{mean(Var)} \tag{4}$$

$$Negative\ decline_p = \frac{mean\left(Var_{-p}\right) - mean(Var)}{mean(Var)} \tag{5}$$

$$AI_p = Positive\ pulse_p - Negative\ decline_p \tag{6}$$

where ***var*** is the yearly value of GPP, NPP, and VOD. ***mean*** represents the mean yearly values. '+p' indicates the replacement of yearly values above the pth percentile with the median value, and '-p' indicates the replacement of yearly values under the (100-p)th percentile with the median value over the averaging period (2003–2018). *Positive pulse*$_p$, corresponding to *Positive pulse* in Eq. (1), indicates that the positive precipitation extremes increase the mean value of variables. *Negative decline*$_p$, corresponding to *Negative decline* in Eq. (2), indicates that the negative precipitation extremes decrease the mean value of variables. $AI_p > 0$ indicates that the increase in mean yearly value of variables due to the positive precipitation extremes is higher than the decrease due to the negative precipitation extremes and vice versa.

In the present study, 20th (p=20) was selected to calculate the asymmetry index based on Haverd method. *Positive pulse* was simply referred as pulse and *Negative decline* was referred as decline. Meanwhile, to study the decadal trends of asymmetry, we used a temporal moving window of 5 years to calculate the running mean of AI.

2.3.2. Drivers of the asymmetry

Previous studies showed that abiotic factors (e.g. precipitation) and biotic factors (e.g. growth potentials of vegetation in response to resource pulses) can have an effect on the asymmetry of vegetation productivity (Al-Yaari et al., 2020; Felton et al., 2021). Also, mean annual precipitation is a key factor in limiting vegetation productivity and its biomass (Huxman et al., 2004). A strong relationship has been reported between vegetation primary productivity and precipitation over Southwest China (Linger et al., 2020; Wu et al., 2013). Therefore, we consider four climatic variables and a biotic variable to explore the possible drivers for the asymmetry of vegetation productivity. These variables include the ratio of yearly precipitation to PET (RATio), the mean annual precipitation (MeanPR), the precipitation interannual variability (CVPR; calculated by the coefficient of variation of precipitation), the asymmetry of precipitation anomalies (AiPR), as well as the productivity potential of vegetation (MaxNPP; calculated by the largest yearly values of NPP).

In the present study, we used the Random Forest (RF) model to determine the most important predictor variable. RF model was an ensemble learning method for classification and regression (Rial et al., 2017), which has advantages in the handling of categorical and continuous predictors, resistance to overfitting, and measurement of variable importance (Iverson et al., 2008). Here, we used the function of "TreeBagger" in RF model based on MATLAB (version R2021a) to estimate the importance of the variables, and used all available pixels of created variable maps over study region as the input variable. We also calculated the variable importance for each biome according to the IGBP land cover map. The above process was repeated 100 times, and selected mean value of all runs as the output result. These variables showing the highest importance could be considered as key drivers for the asymmetry of vegetation productivity.

3. Results

3.1. Biome specific productivity asymmetry

The asymmetry of productivity over Southwest China was quantified for each biome (Fig. 2a-c), and the results from AI_{GPP} (Fig. 2a) and AI_{NPP} (Fig. 2b) showed a negative asymmetry of vegetation productivity in Southwest China, suggesting that the gain of vegetation primary productivity during wet years exceeds the loss during dry years. Across four biomes (e.g., forest, shrublands, grasslands, and croplands), the asymmetry of vegetation productivity was generally negative. The AI_{GPP} value was negative in all biomes, and grasslands had the highest negative AI_{GPP} value (Fig. 2a). AI_{NPP} showed the same negative except for grasslands (Fig. 2b). The AI_{VOD} was negative for grasslands (Fig. 2c). These results showing negative AI values over Southwest China suggest that the decrease in vegetation primary productivity during dry years was, generally, larger than the increase during wet years.

The spatial patterns of AI response over Southwest China showed spatial heterogeneity among GPP (Fig. 2d), NPP (Fig. 2d), and VOD (Fig. 2f). The negative AI_{GPP} and AI_{NPP} values could be observed in the Yunnan province, the western part of Guizhou and Guangxi province, in contrast to the positive AI values over the northwestern Sichuan, southern and northern part of Chongqing, and eastern part of Guizhou. Compared to the spatial patterns of AI_{GPP} and AI_{NPP}, higher negative AI_{VOD} value was observed in the forest regions of Chongqing (Fig. 2f). These results were generally similar to those produced from the Haverd method (Fig. S1).

3.2. Decadal trends of asymmetry

The change in the asymmetry of vegetation productivity in response to precipitation anomalies for a 5 year's temporal moving window from 2003–2018 was investigated (Fig. 3). The negative asymmetry of vegetation primary productivity shifted to positive asymmetry over the study period, indicated by AI_{GPP} (slope=0.000309) and AI_{NPP} (slope=0.000715). For each biome, the decadal trends of asymmetry were similar to overall trend (Fig. S3), although there were differences in the magnitude of change fluctuations among the different biomes. Fluctuations in forests and croplands were relatively small and similar, whereas fluctuations in grasslands and shrublands were larger and the response was more pronounced for grasslands than for shrublands. These results indicate that the sensitivity of vegetation productivity to negative precipitation anomalies during dry years has decreased, which could suggest that the resistance of vegetation to drought has increased even if the frequency of the droughts that occurred over the study period is higher.

A high interannual variability in productivity asymmetry was

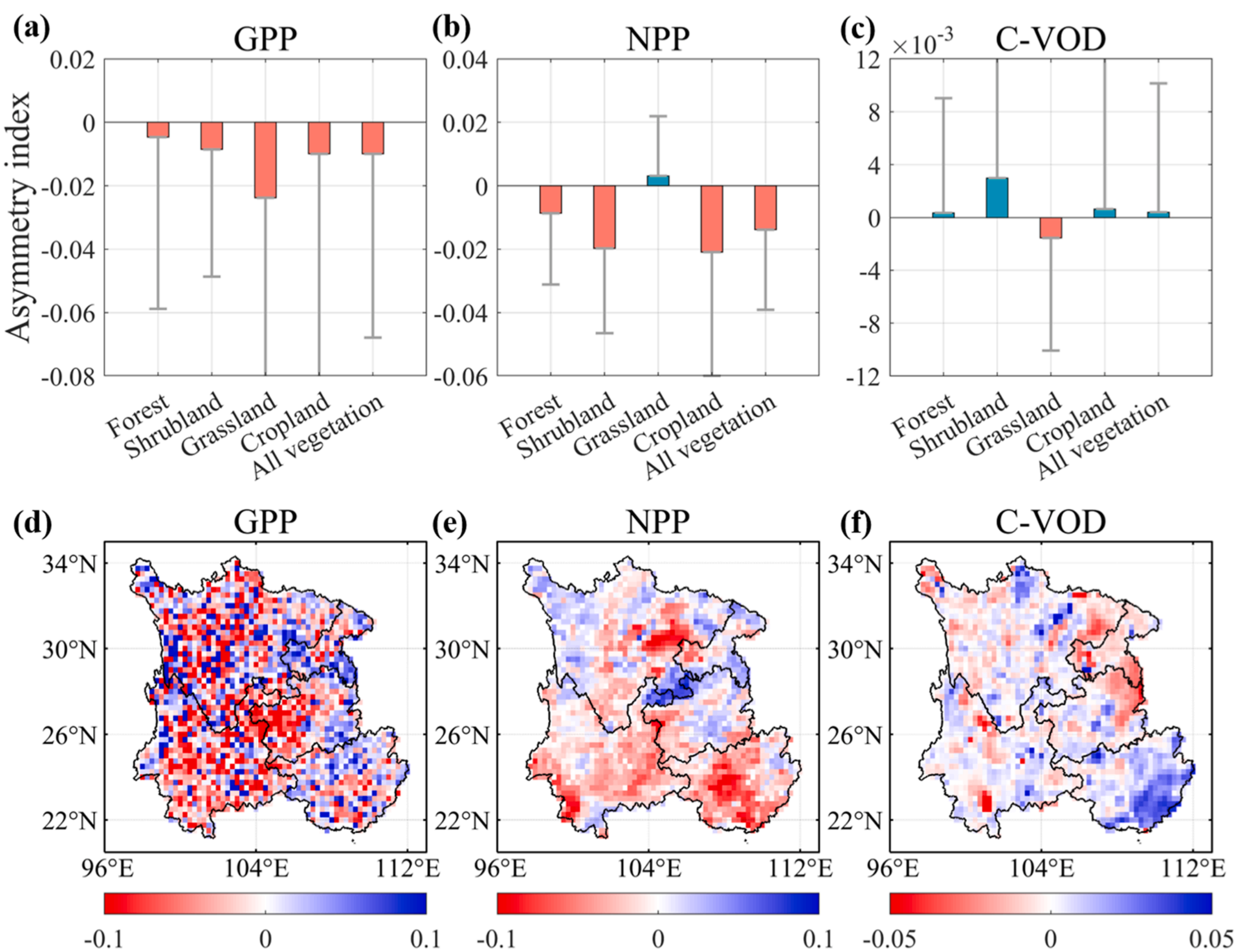

Fig. 2. Asymmetric response of GPP, NPP, and C-VOD to precipitation anomalies in Southwest China. (a)-(c) shows the asymmetry index (AI) of GPP, NPP, and C-VOD for each biome, respectively. (d)-(f) shows the spatial distribution of AI in GPP, NPP, and C-VOD within 2003–2018 period respectively using the method from Al-Yaari et al. (2020).

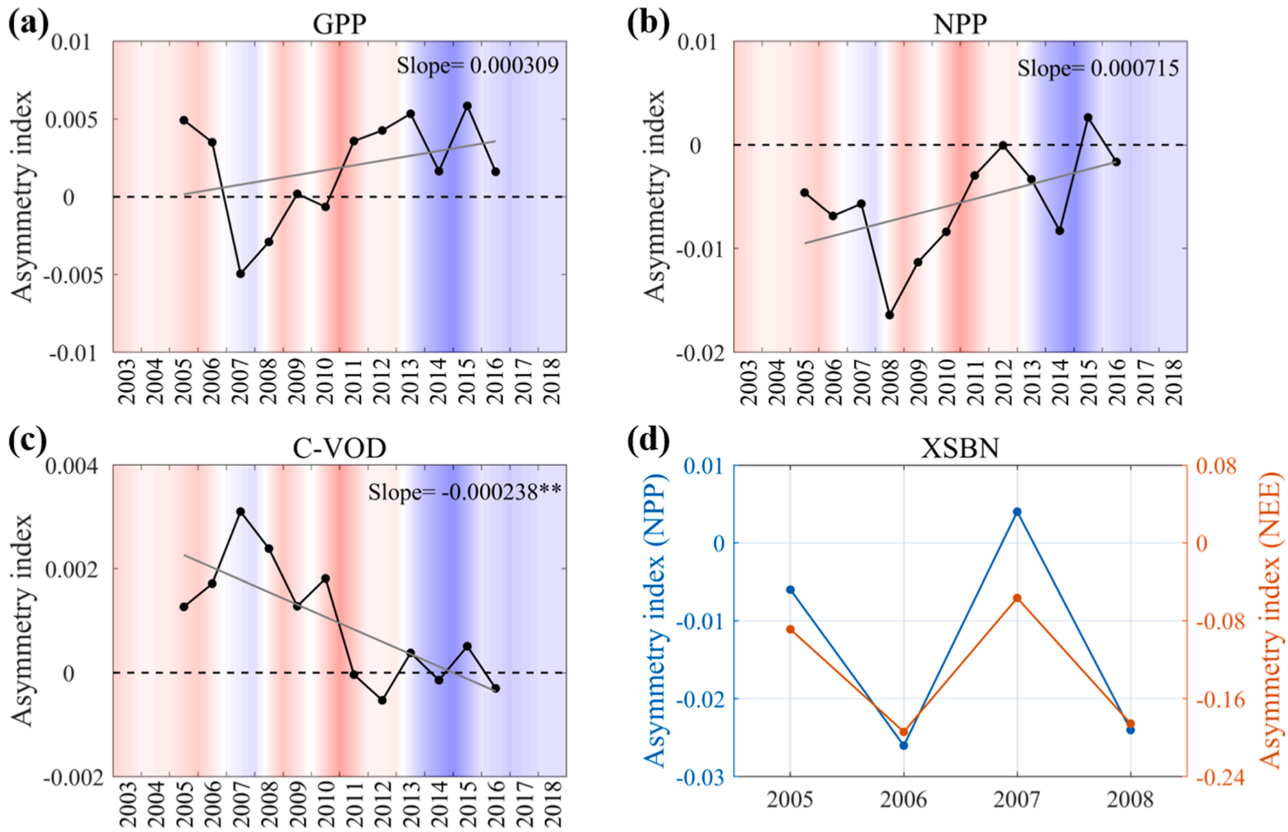

Fig. 3. Temporal variations of the asymmetry index (AI). (a)-(c) represents the asymmetry of GPP, NPP, and C-VOD respectively. (d) shows the asymmetry of NPP product and in-situ NEE measurement at Xishuangbanna (XSBN). The AI is calculated from average interannual variations in vegetation variables using a moving-average window of 5 years using the method from Al-Yaari et al. (2020). The background shading shows the intensity of rainfall anomalies defined by z-score using TerraClimate precipitation, where red/blue color represents the negative/positive z-score values in precipitation, respectively. The gray line represents the long-term trend of AI. ** for $P < 0.01$ and * for $P < 0.05$.

observed during the study period. A downward trend in AI_{GPP} (Fig. 3a) and AI_{NPP} (Fig. 3b) values were observed before 2008, and the strongest negative asymmetries for AI_{GPP} (-0.005) and AI_{NPP} (-0.0164) were observed in 2007 and 2008, respectively. Also, the AI_{GPP} value switched from positive to negative in 2007. These downward trends in AI_{GPP} and AI_{NPP} could be attributed to the long-term seasonal drought during 2003–2014 (Lin et al., 2015). The same trends in AI_{GPP} and AI_{NPP} were similar to those produced from the Haverd method (Fig. S2). Furthermore, to validate the trend of AI_{NPP} at the site scale, we selected one NPP pixel (Fig. 3d), which contained the observed NEE value from XSBN site during the period of 2003–2010. A high agreement (r=0.9956, P-value<0.01) between AI_{NPP} and the in-situ AI_{NEE} was observed from 2005–2008 at XSBN. Also, the XSBN site was in the natural forests of Southwest China (Yu et al., 2006), NPP in forests and NEE fluxes both represented a negative asymmetry over the study period, and declined sharply in 2008 (Fig. S3). These results suggest that drought events (e.g., 2006 summer drought; 2009/2010 winter-spring drought) over Southwest China could affect the asymmetry of vegetation primary productivity, leading to the decrease of vegetation primary productivity during dry years exceeds the increase during wet years.

Note that the increase in the AI_{GPP} was observed after 2007 and switched from negative to positive in 2011, and AI_{NPP} also showed an increase since 2008. However, the AI_{VOD} value decreased after 2007 (Fig. 3c), and experienced a positive to a negative shift in asymmetry in 2011. The AI_{VOD} showed the overall trend of a significant decline (slope<0) during 2003–2018, in contrast to the positive trends in AI_{GPP} and AI_{NPP}.

3.3. Comparison of asymmetric responses for each biome

For a better understanding of the response of vegetation productivity to precipitation anomalies, the method Eq. (1)-(6) for the calculation of the positive pulse and negative decline of productivity was also used to calculate the positive pulse and negative decline of precipitation. The average pulses and declines of productivity and precipitation were grouped by four biomes (forest, shrubland, grassland, and cropland) (Fig. 4). Grasslands were observed to be the most responsive to high precipitation anomalies indicated by the higher positive pulse values (0.1446 for GPP, 0.1092 for NPP), followed by croplands (0.1412 for GPP, 0.0963 for NPP), forests (0.132 for GPP, 0.0808 for NPP) and shrublands (0.1242 for GPP, 0.0781 for NPP). Also, forests and shrublands did not show high values of positive pulse and negative decline compared with grasslands, even experiencing high precipitation anomalies. These results, supported by the results of Haverd method (Fig. S4), indicated that grasslands are more flexible than other biomes and able to adjust primary productivity in response to high precipitation anomalies.

3.4. Drivers for the asymmetry of vegetation primary productivity

The relationship between asymmetry of vegetation productivity and elevation was investigated (Fig. 5). We found the AI_{GPP} and AI_{NPP} values gradually shifted from negative to positive with increasing elevation (Fig. 5a and b), in contrast to AI_{VOD} showed a gradually decreasing trend (Fig. 5c). Both the values of pulse and decline showed decreasing trends between 0 and 2500 m, and an increasing trend between 2500 and 4500 m (Fig. 5d-f). In general, the minimum values of these two pulses can be observed at elevations between 2000 and 3000 m, and the maximum

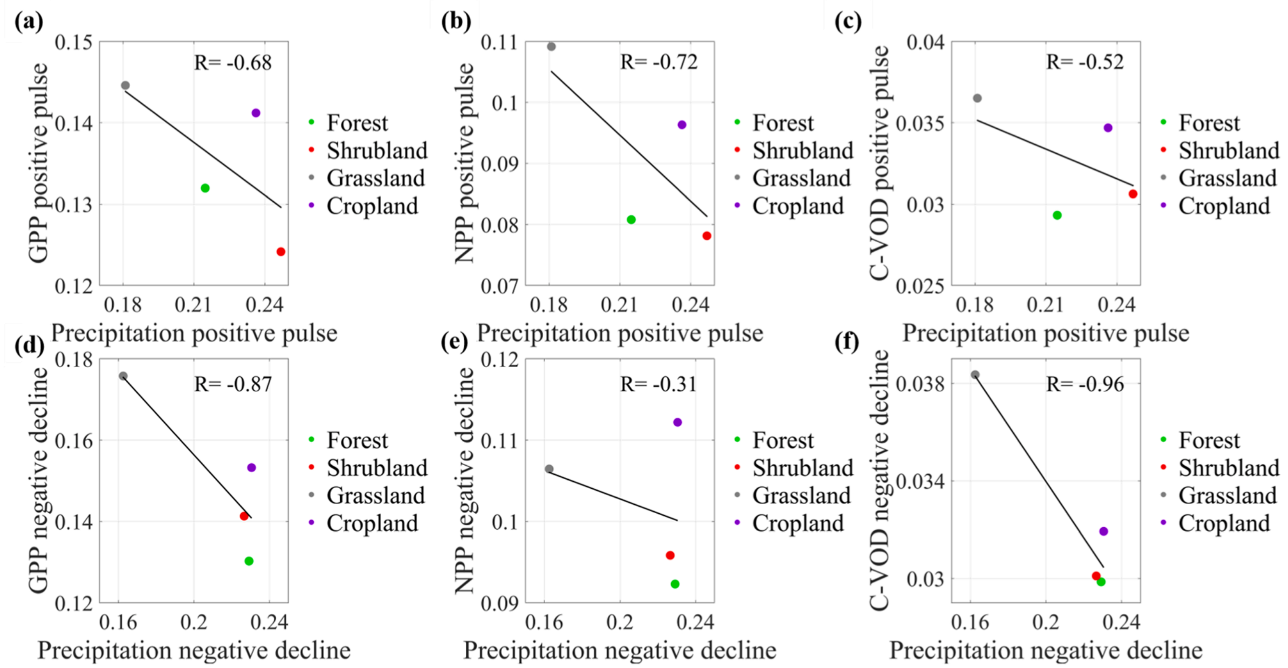

Fig. 4. The sensitivity of GPP, NPP, and C-VOD to precipitation anomalies for each biome. The axis of (a)-(c) represents the positive pulse of GPP, NPP, and C-VOD, respectively. The axis of (d)-(f) represents the negative decline of GPP, NPP, and C-VOD, respectively. The positive and negative pulses were calculated using the method from Al-Yaari et al. (2020). The same method was used to calculate the positive pulse and negative decline of precipitation.

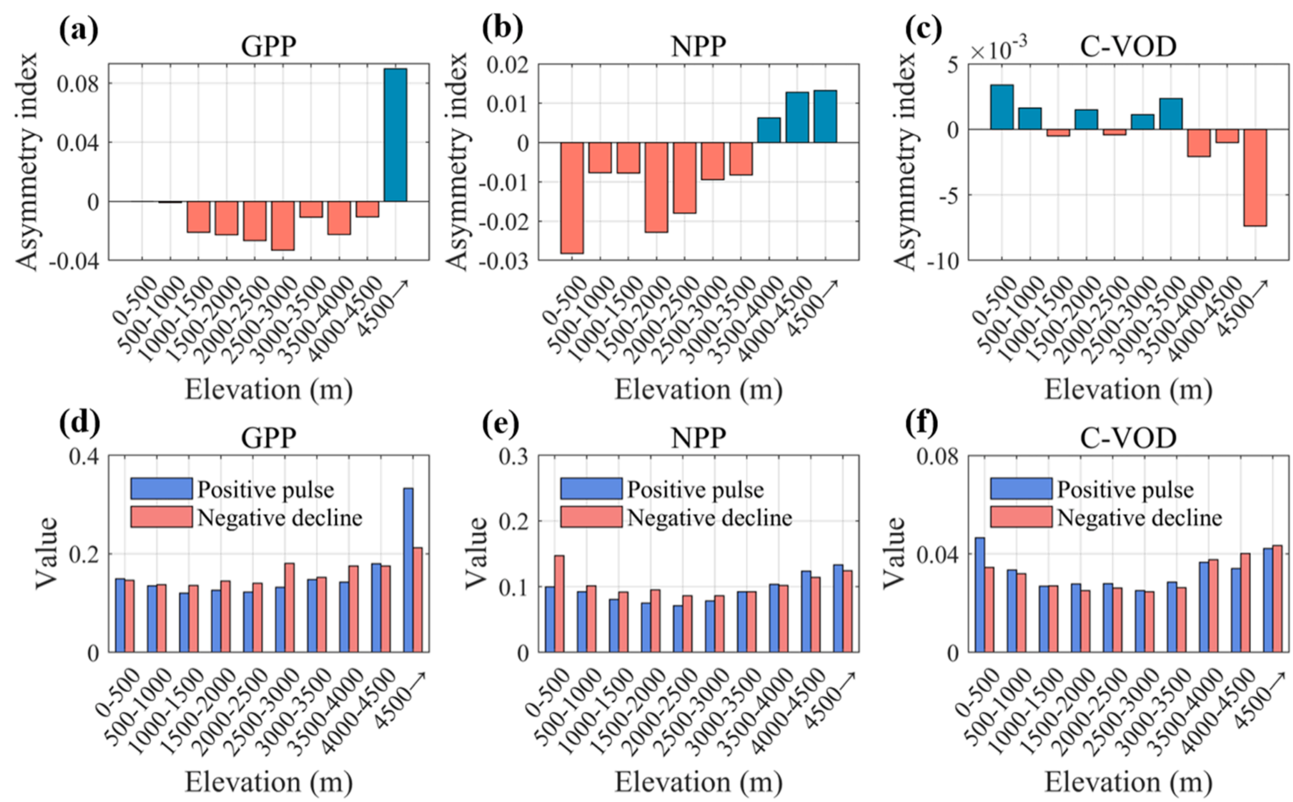

Fig. 5. The influence of elevation on the asymmetry of vegetation productivity. The relative magnitude of (a)-(c) the asymmetry index and (d)-(f) positive pulses and negative declines for GPP, NPP, and C-VOD for different elevation conditions, respectively. The asymmetry index, positive pulse, and negative decline were calculated using the method from Al-Yaari et al. (2020).

value can be observed above 4500 m. These results indicate an AI dependency of elevation: more positive AI values occur in areas of high elevation, and more negative AI values occur in areas of low elevation.

The relationship between asymmetry of vegetation productivity and temperature was investigated (Fig. 6). We found an AI_{GPP} value corresponding negative asymmetry below 30 °C (Fig. 6b), in contrast to the

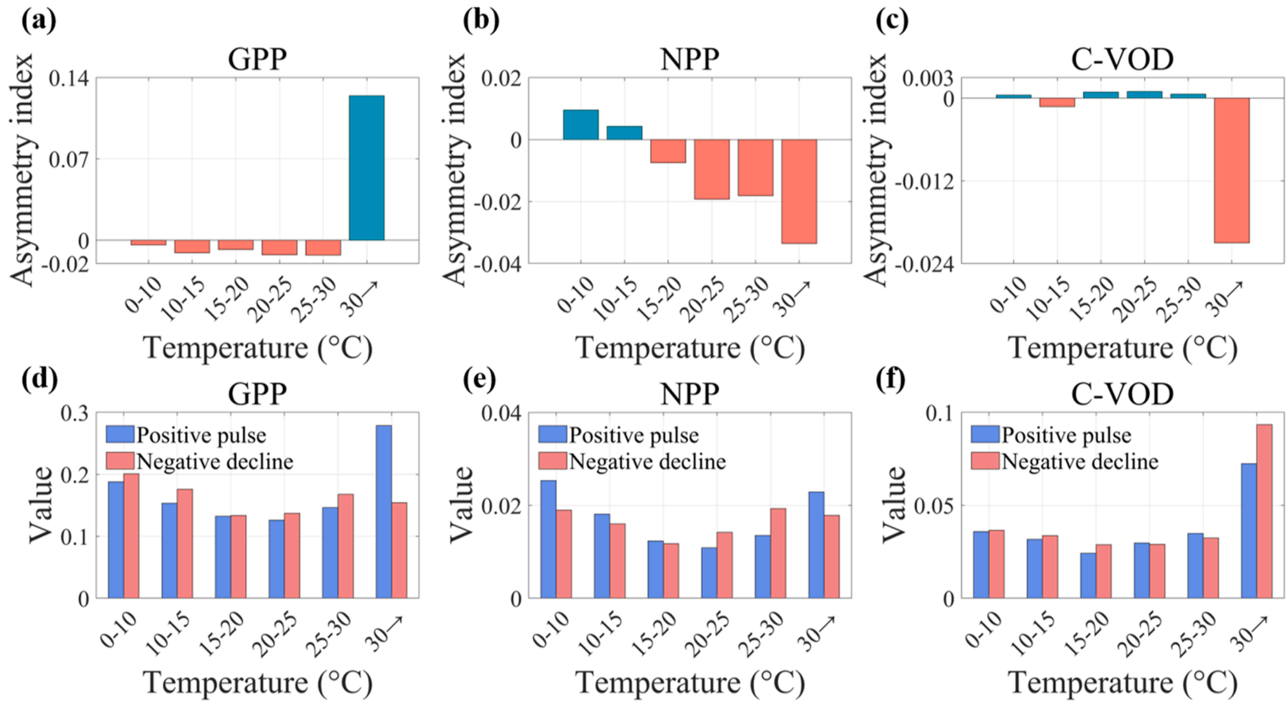

Fig. 6. The influence of temperature on the asymmetry of vegetation productivity. The relative magnitude of (a)-(c) the asymmetry index and (d)-(f) positive pulses and negative declines for GPP, NPP, and C-VOD for different temperature conditions, respectively. The asymmetry index, positive pulse, and negative decline were calculated using the method from Al-Yaari et al. (2020).

AI_{VOD} showing positive asymmetry (Fig. 6c), and the AI_{NPP} value gradually shifted from positive to negative as a function of increasing temperature (Fig. 6a). Both values of pulse and decline showed decreasing trends between 0 °C and 20 °C, and an increasing trend between 20 °C and above 30 °C (Fig. 6d-f). The minimum values of these two pulses can be observed at temperatures between 15 °C and 25 °C, and the maximum value can be observed above 30 °C. The result of AI_{NPP} indicates that high temperatures have a strong influence on the asymmetry of vegetation productivity, causing strongly negative AI_{NPP} in areas with high temperatures. These results were generally similar to those produced from the Haverd method (Fig. S5 and Fig. S6).

The relationship between the asymmetry of vegetation productivity

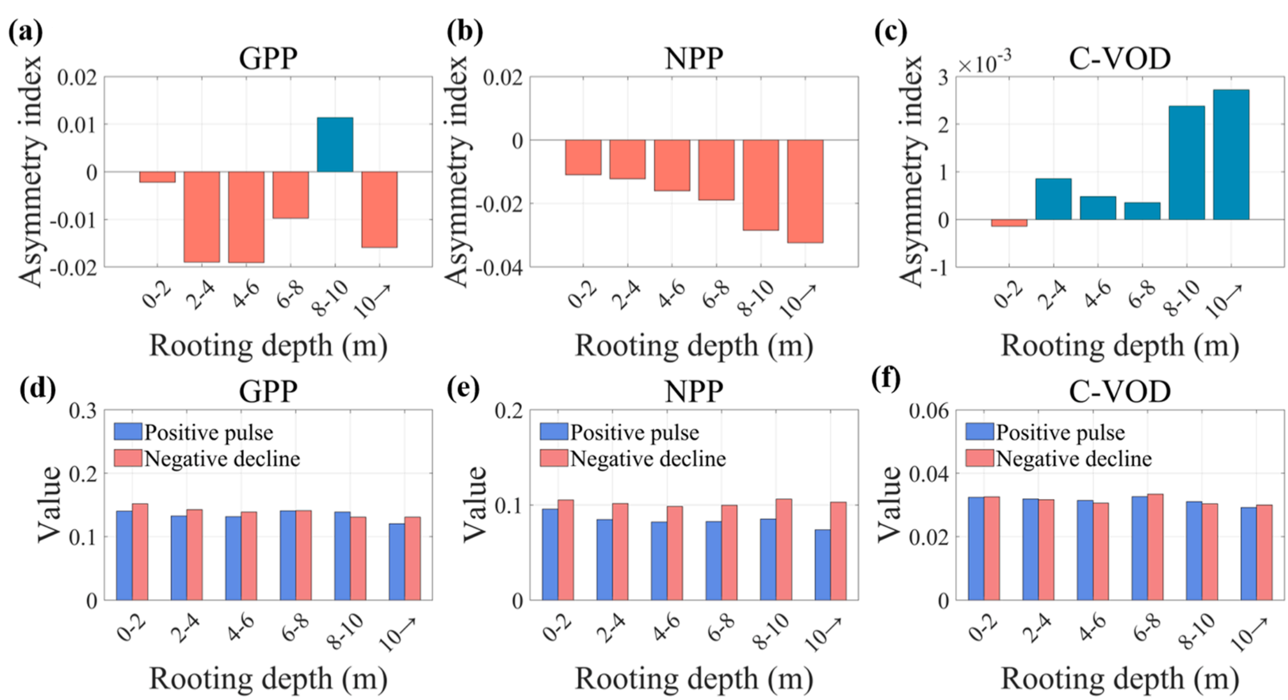

Fig. 7. The influence of maximum rooting depth on the asymmetry of vegetation productivity. The relative magnitude of (a)-(c) the asymmetry index and (d)-(f) positive pulses and negative declines for GPP, NPP, and C-VOD for different maximum rooting depth conditions, respectively. The asymmetry index, positive pulse, and negative decline were calculated using the method from Al-Yaari et al. (2020).

and maximum rooting depth was studied (Fig. 7). There are no significant trends in positive pulse and negative decline values with increasing rooting depth (Fig. 7d-f), suggesting that the vegetation in this region is not under severe water stress and that vegetation is not primarily controlled by precipitation despite the presence of karst landscape structure in this region.

In addition, five variables with the RF models were used to predict the asymmetry of vegetation productivity (Fig. 8). These results showed that RATio was the most important predictor variable in AI_{GPP}, MaxNPP was the most important indicator in AI_{NPP} followed by MeanPR which was the most important indicator in AI_{VOD} (Fig. 8a). At the biome scale, RATio, MaxNPP, and MeanPR were the most important indicators in forests areas for AI_{GPP} (Fig. 8b), AI_{NPP} (Fig. 8c), and AI_{VOD} (Fig. 8d), respectively. MeanPR was the most important indicator in shrublands, suggesting that productivity asymmetry over shrublands could be explained by the mean annual precipitation. RATio, MeanPR, and MaxNPP were the most important indicators for grasslands in AI_{GPP}, AI_{NPP}, and AI_{VOD} respectively. MeanPR was the most important indicator for grasslands in AI_{NPP} and AI_{VOD}.

4. Discussion

4.1. Asymmetric response of vegetation productivity to precipitation anomalies

These results indicated that vegetation productivity over Southwest China showed negative asymmetry between 2003 and 2018 (Fig. 2), in contrast to previous studies on arid and semi-arid regions (Haverd et al., 2017). Our studies emphasize on the dominant role of negative asymmetry of vegetation productivity in Southwest China, suggesting that vegetation in this region is vulnerable to drought events. These results characterizing humid regions were in line with site-scale studies over the grassland site located in the Austrian Central Alps (Wu et al., 2018). The negative AI value could be caused by a situation where an increase in vegetation productivity during wet years could not compensate for the decline of vegetation productivity due to the frequent drought. In extreme wet years, vegetation productivity over the humid regions tends to saturate or decline with increased precipitation, concurrent with the reduction in other available resources such as light and nutrients (Schwalm et al., 2010). At the same time, the temperature and radiation, as key factors for vegetation growth, may alter with the duration of rainy periods, thus negatively affecting vegetation primary productivity (Nemani et al., 2003). On the contrary, during extreme drought years, vegetation primary productivity decreases significantly with continued reduction in precipitation (Yuan et al., 2016). In particular, dramatic declines in vegetation productivity may occur when precipitation decreases exceed the threshold of vegetation mortality (McDowell et al., 2011). Furthermore, additional negative effects such as heatwaves, fire disturbance (Qin et al., 2022), and pest breakout (Brando et al., 2014) could also reduce vegetation productivity.

The AI_{VOD} value was positive among three biomes of forest, croplands, and shrublands (except for grassland), which was opposite to the results of AI_{NPP}. There are two potential reasons to explain the unexpected opposite result between AI_{VOD} and AI_{NPP}. The first reason may be due to the oversimplification of the passive microwave VOD retrieval algorithms (Wang et al., 2023), which could result in an overestimation of VOD during dry years. A recent evaluation study (Wang et al., 2023) based on multiple VOD products showed a negative correlation between the VODCA C-VOD and soil moisture in Amazon forests, and attributed it to the simplified scattering process and inappropriate parameter setting in VOD retrieval algorithms. In addition, MODIS NPP, as an optical remote sensing product, could be affected by cloud contamination, topography, and aerosol concentrations (Zeng et al., 2022), leading to a decrease in the accuracy of the NPP product. The other reason could be related to the anthropogenic factors such as intensive afforestation ecological protection that promoted the growth of vegetation in Southwest China after 2000. A previous study showed that large-scale ecological projects in Southwest China have led to a broad increase in the leaf area index (LAI) and AGB, which attenuated the negative effects caused by drought, resulting in an overall positive asymmetry in biomass in this region during 2003–2018 (Tong et al., 2020; Tong et al., 2017).

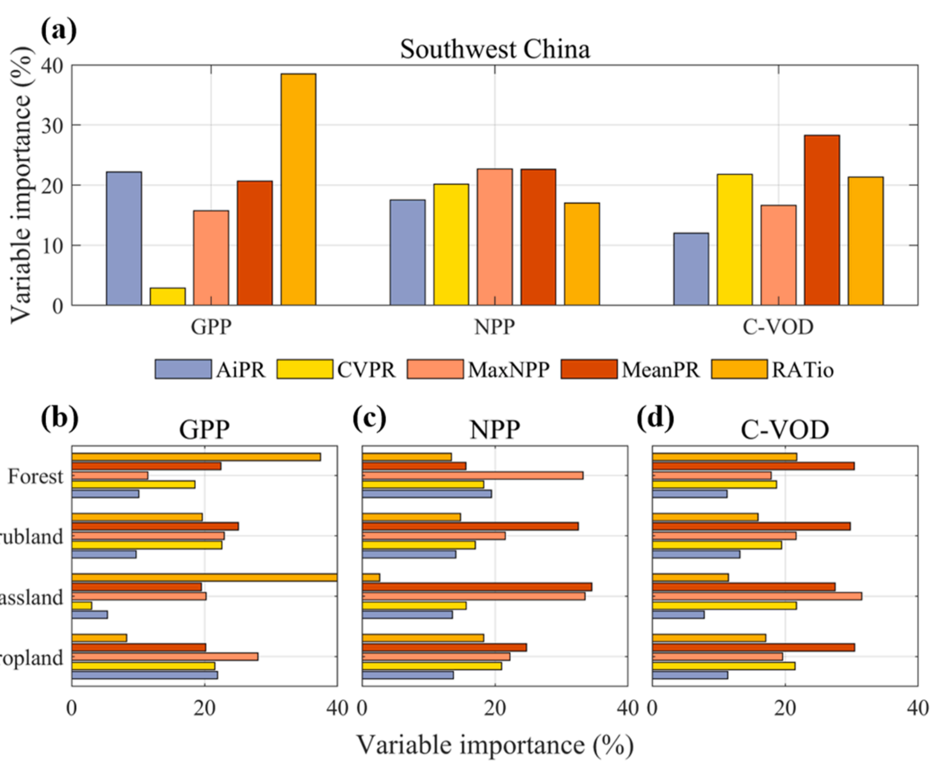

Fig. 8. Variable importance of the five predictors used to predict the asymmetry of vegetation productivity. High values indicate more important drivers in RF models. (a) shows the variable importance of predictors used to predict the asymmetry index of GPP, NPP, and C-VOD across entire Southwest China, respectively. (b)-(d) shows the variable importance of predictors used to predict the asymmetry index of GPP, NPP, and C-VOD for each biome, respectively. The input variables were the ratio of yearly precipitation to potential evapotranspiration (RATio), mean annual precipitation (MeanPR), precipitation interannual variability (CVPR), asymmetry of precipitation anomalies (AiPR), and productivity potential of vegetation (MaxNPP), respectively.

4.2. Comparison of the asymmetric response for each biome

Our results showed that vegetation productivity from grasslands had the highest sensitivity to precipitation anomalies (Fig. 4), suggesting that the primary productivity in grasslands is more susceptible to precipitation anomalies than in other biomes. Grasslands with high sensitivity to drought have a simpler structure and lower productivity compared to forests and shrublands, with aboveground parts that tend to wither during drought periods but re-emerge rapidly when drought ceases to occur. (Stampfli et al., 2018). Furthermore, while grasslands regrow rapidly as precipitation deficits alleviate, those grasslands usually do not immediately restore to pre-drought productivity states of carbon sequestration (Stuart-Haentjens et al., 2018), which may also explain why the grassland's primary productivity shows negative asymmetry. Our result differs from a meta-analysis of grassland precipitation manipulation experiments at dry sites (Wilcox et al., 2017) that found a positive asymmetry of vegetation productivity in response to precipitation extremes. This could reveal an interesting difference between grassland functioning out study region (mainly belong to humid regions) in contrast to findings of (semi-)arid regions, that grassland primary productivity in humid regions is more susceptible to the effects of dry years relative to wet years.

Forests showed relatively weaker negative asymmetric response to precipitation anomalies, suggesting that forests have a stronger capability of drought resistance than crops and grasslands (Li et al., 2019). At the early stage of the drought period, forests could absorb precipitation held in the root zone or shallow soil moisture (Liu et al., 2019). Compared with other three biomes, even under high water deficit conditions, forests could be able to adjust stomatal conductance and reduce transpiration to avoid excessive water loss (Choat et al., 2018; Reichstein et al., 2002).

Compared with grasslands and forests, shrublands have a moderate sensitivity to precipitation anomalies and recovery time for vegetation productivity, due to their more complex structure and function than grasslands and less demand for water, nutrients, and carbohydrates for growth than forests (Li et al., 2019). In contrast to natural biomes, cropland may have water supplements like artificial irrigation and cultivation and thereby be less sensitive to increase in precipitation, showing negative asymmetric response to precipitation anomalies. These results were in line with a recent study from Wang et al. (2022) who found a significant negative AI in croplands.

4.3. Effect of precipitation anomalies on vegetation productivity asymmetry

Our results also showed that the AI_{GPP} and AI_{NPP} values shifted from negative to positive over the study period (Fig. 3), although persistent negative precipitation anomalies and drought events occurred between 2003 and 2014. This may be due to the intrinsic response of the vegetation mediates or buffers the cumulative negative effects over time (Felton et al., 2021), resulting in a diminished rather than amplified negative asymmetric response of vegetation productivity. For instance, a recent study (Trugman et al., 2020) found evidence of a shift towards forests with more drought-tolerant traits, driven by forest mortality. Furthermore, long-term drought can select for species with drought resistance and lead to changes in species composition (Fauset et al., 2012), thus weakening the negative response of vegetation productivity to precipitation anomalies (Felton and Smith, 2017; Jentsch et al., 2011).

Surprisingly, the 2011 summer drought attenuates the negative asymmetry of productivity in forest despite a significant reduction in precipitation (Fig. S3). This could be due to the increase in incoming solar radiation available to vegetation in 2011, resulting in an increase in primary productivity. A study by (Song et al., 2019) indicates that the incoming solar radiation increased by 13% during the 2011 summer drought because of cloud cover reduction, which facilitated the vegetation growth in the case where water is not limited. The increase in solar radiation contributed to the greening of the forest and the increase in canopy photosynthesis, although this region experienced a reduction in precipitation during the summer drought in 2011 (Song et al., 2019). Similar findings could be found in the Amazon forest (Jones et al., 2014; Yang et al., 2018) that due to the increase in solar radiation in Amazon forests, the extreme drought in 2015–2016 did not affect the greenness of vegetation and even promoted the growth of vegetation.

4.4. Influencing factors for the asymmetry of vegetation primary productivity

The AI_{GPP} and AI_{NPP} values gradually shifted from negative to positive with increasing elevation (Fig. 5), indicating that the elevation is a strong factor for the asymmetry of vegetation productivity over these humid regions. The positive AI values at high altitudes could be caused by that relatively strong incoming solar radiation. In this region, the average temperature and precipitation drop as the elevation increase (Tong et al., 2016). In dry years, strong incoming solar radiation enhanced vegetation growth and offset the negative effects of water deficits. Thus, vegetation primary productivity in areas of high elevation was more responsive to wetter conditions, showing positive AI values.

Plant rooting depth could affect the resilience of vegetation to drought (Fan et al., 2017). However, the positive pulse and negative decline varied little within different root depths (Fig. 7), which is different from that found by Al-Yaari et al. (2020). This may be caused by the fact that precipitation in humid regions (e.g., Southwest China) can meet the demands of vegetation growth (Chen et al., 2021) despite the presence of karst landforms in this region.

4.5. Uncertainties

Our research still has potential deficiencies and limitations related to the datasets used:

(1) The uncertainties of NPP and GPP products: the accuracy of remote sensing products is affected by topography (Zeng et al., 2022), which could cause shadows and alter the geometry of the local sun-surface-sensor. For example, EVI, as the input parameter of the VPM model to calculate GPP, could be affected by the dark and opaque topographic shadows (Matsushita et al., 2007). Also, cloud and aerosol effects are responsible for the decrease in high-quality observations. For example, LAI, as the key input for the NPP product, was subject to uncertainties in atmospheric correction, such as cloud masking, residual sub-pixel clouds, incomplete corrections for water vapor absorption, and aerosol (Zeng et al., 2022). Thus, high-quality and high-resolution (e.g., 10-m spatial resolution) vegetation products will be helpfully understand the asymmetric response of vegetation productivity to precipitation anomalies.

(2) The uncertainty of the C-band VOD product: For the C-VOD values, biomass increases non-linearly with VOD, but prone to saturation at high biomass values (Liu et al., 2015). This is because the higher-frequency C-VOD values are sensitive to the top of the canopy and leaf biomass (Liu et al., 2013; Liu et al., 2018; Tian et al., 2017), potentially affecting the accuracy of AI_{VOD} value. L-VOD indices are more sensitive to the entire vegetation stratum (including leaves, branches and trunks), which is not the case for high-frequency. However, the period covered by passive microwave instruments operating in the L-band is too short to be applied in the study. Additionally, the coarse spatial resolution (e.g., 25-km) of the VOD product limited its applicability for assessing the asymmetry of vegetation productivity at a finer scale, and C-band VOD was affected by strong radio frequency interference (Frappart et al., 2020). Furthermore, multiple land cover types (e.g., forests, croplands, and

grasslands) were often mixed within a single 25-km pixel. The coarse spatial resolution therefore posed challenges for accurately calculating a representative AI value for each biome. Higher spatial resolution VOD products will be needed for future research in this direction.

Although extreme drought events could affect the asymmetry of vegetation productivity over Southwest China, our results did not consider whether the frequency of drought events would have an impact on vegetation productivity asymmetries. In fact, previous studies (Dannenberg et al., 2019; Knapp et al., 2017) have reported that the increase in precipitation variability could suppress forest growth and lead to a negative asymmetry of vegetation productivity in response to precipitation anomalies. Thus, the negative asymmetry of vegetation productivity may be more pronounced in areas with a higher frequency of drought events. Our study mainly selected Al-Yaari method to analyzed possible asymmetric response of vegetation productivity to precipitation anomalies over Southwest China. Due to the limited study period, our results lacked a comprehensive analysis toward the asymmetric response of vegetation productivity to extreme precipitation. Further study should use long-term vegetation productivity datasets to explore vegetation productivity asymmetry under extreme climate.

5. Conclusion and outlook

We evaluated the asymmetry of vegetation productivity in response to precipitation anomalies with an asymmetry index (AI) over Southwest China from 2003 to 2018, and found a negative asymmetry of vegetation productivity, with the vegetation productivity losses during dry years exceeding the gains during wet years. The AI of VOD showed positive asymmetry, partly being attributed to a series of ecological conservation projects implemented in Southwest China. Large-scale ecological conservation projects, such as intensive afforestation and reforestation projects, could be able to increase the LAI and AGB, attenuating the negative effects of vegetation caused by drought. Furthermore, the asymmetry of vegetation primary productivity shifted during the period of analysis towards positive asymmetry, although drought events frequently occurred over the study period, suggesting that the sensitivity of vegetation productivity to negative precipitation anomalies in dry years has decreased and the resistance of vegetation to drought has increased. Vegetation productivity from grasslands had the highest sensitivity to precipitation anomalies, suggesting that the productivity of grasslands is more susceptible to precipitation anomalies than other biomes.

Some uncertainties among the datasets in the analysis should be noted, e.g., the effects of atmosphere and topography on the NPP and GPP products, and the saturation effect on C-VOD. For better understand the ecosystem function under climate change, the potential mechanisms of asymmetric response for each biome in humid areas should be further investigated. Extended time series and high spatial resolution vegetation productivity products and L-band VOD products should be used in the future.

Data availability statement

The MODIS land cover data are available at: https://doi.org/10.5067/MODIS/MCD12Q1.006. The MODIS NPP data can be downloaded from: https://doi.org/10.5067/MODIS/MOD17A3HGF.006. The MODIS LST data are available at: https://doi.org/10.5067/MODIS/MOD11A1.006. The NASA SRTM elevation data can be derived from: https://doi.org/10.1029/2005RG000183. The TerraClimate PET and precipitation data can be downloaded from: https://www.nature.com/articles/sdata2017191#citeas. The in situ China FLUX NEE data can be downloaded from: http://www.chinaflux.org/general/index.aspx?nodeid=12. The VPM GPP data can be download at https://drive.google.com/file/d/1ugbUCz1t10nf7iD00yQOBLYyrlRXiY96/view. The VODCA VOD data can be download at https://zenodo.org/record/2575599#.Y05xuTFByUm. The maximum rooting depth data can be download from https://wci.earth2observe.eu/thredds/catalog/usc/root-depth/catalog.html.

Declaration of competing interest

The authors declare that they have no known competing financial interests or personal relationships that could have appeared to influence the work reported in this paper.

Data availability

Data will be made available on request.

Acknowledgments

This study is supported in part by research grants from the National Natural Science Foundation of China (Grant No. 42171339,41830648), the Fundamental Research Funds for the Central Universities (SWU020016).

Supplementary materials

Supplementary material associated with this article can be found, in the online version, at doi:10.1016/j.agrformet.2023.109350.

References

Abatzoglou, J.T., Dobrowski, S.Z., Parks, S.A., Hegewisch, K.C., 2018. TerraClimate, a high-resolution global dataset of monthly climate and climatic water balance from 1958-2015. Sci. Data 5, 170191.
Al-Yaari, A., et al., 2020. Asymmetric responses of ecosystem productivity to rainfall anomalies vary inversely with mean annual rainfall over the conterminous United States. Glob. Chang Biol. 26 (12), 6959–6973.
Brando, P.M., et al., 2014. Abrupt increases in Amazonian tree mortality due to drought-fire interactions. Proc. Natl. Acad. Sci. U.S.A. 111 (17), 6347–6352.
Brandt, M., et al., 2018. Satellite-observed major greening and biomass increase in South China karst during recent decade. Earth's Future 6 (7), 1017–1028.
Chen, X., et al., 2021. The ongoing greening in Southwest China despite severe droughts and drying trends. Remote Sens. 13 (17), 3374.
Choat, B., et al., 2018. Triggers of tree mortality under drought. Nature 558 (7711), 531–539.
Dannenberg, M.P., Wise, E.K., Smith, W.K., 2019. Reduced tree growth in the semiarid United States due to asymmetric responses to intensifying precipitation extremes. Sci. Adv. 5 (10), eaaw0667.
Fan, Y., Miguez-Macho, G., Jobbagy, E.G., Jackson, R.B., Otero-Casal, C., 2017. Hydrologic regulation of plant rooting depth. Proc. Natl. Acad. Sci. U.S.A., 114 (40), 10572–10577.
Farr, T.G., et al., 2007. The shuttle radar topography mission. Rev. Geophys. 45 (2), RG2004.
Fauset, S., et al., 2012. Drought-induced shifts in the floristic and functional composition of tropical forests in Ghana. Ecol. Lett. 15 (10), 1120–1129.
Felton, A.J., Knapp, A.K., Smith, M.D., 2021. Precipitation-productivity relationships and the duration of precipitation anomalies: An underappreciated dimension of climate change. Glob. Chang Biol. 27 (6), 1127–1140.
Felton, A.J., Smith, M.D., 2017. Integrating plant ecological responses to climate extremes from individual to ecosystem levels. Philos. Trans. R. Soc. Lond. B Biol. Sci. 372 (1723), 20160142.
Frank, D., et al., 2015. Effects of climate extremes on the terrestrial carbon cycle: concepts, processes and potential future impacts. Glob. Chang Biol. 21 (8), 2861–2880.
Frappart, F., et al., 2020. Global monitoring of the vegetation dynamics from the vegetation optical depth (VOD): a review. Remote Sens. 12 (18), 2915.
Ge, W., Han, J., Zhang, D., Wang, F., 2021. Divergent impacts of droughts on vegetation phenology and productivity in the Yungui Plateau, southwest China. Ecol. Indicator. 127, 107743.
Hao, C., Zhang, J., Yao, F., 2015. Combination of multi-sensor remote sensing data for drought monitoring over Southwest China. Int. J. Appl. Earth Obs. 35, 270–283.
Haverd, V., Ahlstrom, A., Smith, B., Canadell, J.G., 2017. Carbon cycle responses of semi-arid ecosystems to positive asymmetry in rainfall. Glob. Chang Biol. 23 (2), 793–800.
Haverd, V., Smith, B., Trudinger, C., 2016. Dryland vegetation response to wet episode, not inherent shift in sensitivity to rainfall, behind Australia's role in 2011 global carbon sink anomaly. Glob. Chang Biol. 22 (7), 2315–2316.
Huxman, T.E., et al., 2004. Precipitation pulses and carbon fluxes in semiarid and arid ecosystems. Oecologia 141 (2), 254–268.

Iverson, L.R., Prasad, A.M., Matthews, S.N., Peters, M., 2008. Estimating potential habitat for 134 eastern US tree species under six climate scenarios. Forest Ecol. Manag. 254 (3), 390–406.
Jentsch, A., et al., 2011. Climate extremes initiate ecosystem-regulating functions while maintaining productivity. J. Ecol. 99 (3), 689–702.
Jones, M.O., Kimball, J.S., Nemani, R.R., 2014. Asynchronous Amazon forest canopy phenology indicates adaptation to both water and light availability. Environ. Res. Lett. 9 (12), 124021.
Knapp, A.K., Ciais, P., Smith, M.D., 2017. Reconciling inconsistencies in precipitation-productivity relationships: implications for climate change. New Phytol. 214 (1), 41–47.
Konings, A.G., Holtzman, N.M., Rao, K., Xu, L., Saatchi, S.S., 2021. Interannual variations of vegetation optical depth are due to both water stress and biomass changes. Geophys. Res. Lett. 48 (16), e2021GL095267.
Laamrani, A., et al., 2014. Effects of topography and thickness of organic layer on productivity of black spruce boreal forests of the Canadian Clay Belt region. Forest Ecol. Manag. 330, 144–157.
Li, X., et al., 2019. The impact of the 2009/2010 drought on vegetation growth and terrestrial carbon balance in Southwest China. Agr. Forest. Meteorol. 269-270, 239–248.
Li, Y., Ren, F., Li, Y., Wang, P., Yan, H., 2014. Characteristics of the regional meteorological drought events in Southwest China during 1960–2010. J. Meteorologic. Res. 28 (3), 381–392.
Li, Y., Xu, H., Liu, D., 2011. Features of the extremely severe drought in the east of Southwest China and anomalies of atmospheric circulation in summer 2006. Acta Meteorologica Sinica 25 (2), 176–187.
Lin, W., Wen, C., Wen, Z., Gang, H.J.A., Letters, O.S., 2015. Drought in Southwest China: a review. Atmos. Oceanic Sci. Lett. 8 (6), 339–344.
Linger, E., et al., 2020. Precipitation influences on the net primary productivity of a tropical seasonal rainforest in Southwest China: A 9-year case study. Forest Ecol. Manag. 467, 118153.
Liu, C.-C., Liu, Y.-G., Fan, D.-Y., Guo, K., 2012. Plant drought tolerance assessment for re-vegetation in heterogeneous karst landscapes of southwestern China. Flora: Morphol. Distribut. Funct. Ecol. Plants 207 (1), 30–38.
Liu, C., et al., 2011a. Effect of drought on pigments, osmotic adjustment and antioxidant enzymes in six woody plant species in karst habitats of southwestern China. Environ. Exp. Botany 71 (2), 174–183.
Liu, C., et al., 2016. Aboveground carbon stock, allocation and sequestration potential during vegetation recovery in the karst region of southwestern China: A case study at a watershed scale. Agric. Ecosyst. Environ. 235, 91–100.
Liu, J., et al., 2019. Response of plants water uptake patterns to tunnels excavation based on stable isotopes in a karst trough valley. J. Hydrol. 571, 485–493.
Liu, Y.Y., de Jeu, R.A.M., McCabe, M.F., Evans, J.P., van Dijk, A.I.J.M., 2011b. Global long-term passive microwave satellite-based retrievals of vegetation optical depth. Geophys. Res. Lett. 38 (18), L18402.
Liu, Y.Y., et al., 2015. Recent reversal in loss of global terrestrial biomass. Nature Climate Change 5 (5), 470–474.
Liu, Y.Y., van Dijk, A.I.J.M., McCabe, M.F., Evans, J.P., de Jeu, R.A.M., 2013. Global vegetation biomass change (1988-2008) and attribution to environmental and human drivers. Glob. Ecol. Biogeogr. 22 (6), 692–705.
Liu, Y.Y., et al., 2018. Enhanced canopy growth precedes senescence in 2005 and 2010 Amazonian droughts. Remote Sens. Environ. 211, 26–37.
Long, D., et al., 2014. Drought and flood monitoring for a large karst plateau in Southwest China using extended GRACE data. Remote Sens. Environ. 155, 145–160.
Loveland, T.R., Belward, A.S., 1997. The international geosphere biosphere programme data and information system global land cover data set (DISCover). Acta Astronaut. 41 (4-10), 681–689.
Matsushita, B., Yang, W., Chen, J., Onda, Y., Qiu, G., 2007. Sensitivity of the enhanced vegetation index (EVI) and normalized difference vegetation index (NDVI) to Topographic effects: a case study in high-density cypress forest. Sensors 7 (11), 2636–2651.
McDowell, N.G., et al., 2011. The interdependence of mechanisms underlying climate-driven vegetation mortality. Trends Ecol. Evol. 26 (10), 523–532.
Moesinger, L., et al., 2020. The global long-term microwave vegetation optical depth climate archive (VODCA). Earth Syst. Sci. Data 12 (1), 177–196.
Nemani, R.R., et al., 2003. Climate-driven increases in global terrestrial net primary production from 1982 to 1999. Science 300 (5625), 1560–1563.
Pei, Y., et al., 2020. Performance of four state-of-the-art GPP products (VPM, MOD17, BESS and PML) for grasslands in drought years. Ecol Inform 56, 101052.
Piao, S., et al., 2009. The carbon balance of terrestrial ecosystems in China. Nature 458 (7241), 1009–1013.
Qin, Y., et al., 2022. Large loss and rapid recovery of vegetation cover and aboveground biomass over forest areas in Australia during 2019–2020. Remote Sens. Environ. 278, 113087.
Ratzmann, G., Gangkofner, U., Tietjen, B., Fensholt, R., 2016. Dryland vegetation functional response to altered rainfall amounts and variability derived from satellite time series data. Remote Sens. 8 (12), 1026.
Reichstein, M., et al., 2002. Severe drought effects on ecosystem CO2 and H2O fluxes at three Mediterranean evergreen sites: revision of current hypotheses? Global Change Biol. 8 (10), 999–1017.
Rial, M., Martinez Cortizas, A., Rodriguez-Lado, L., 2017. Understanding the spatial distribution of factors controlling topsoil organic carbon content in European soils. Sci. Total Environ. 609, 1411–1422.
Running, S., Zhao, M., 2019. MOD17A3HGF MODIS/Terra Net Primary Production Gap-Filled Yearly L4 Global 500m SIN Grid V006[Dataset]. NASA EOSDIS Land Processes DAAC. https://doi.org/10.5067/MODIS/MOD17A3HGF.006. Accessed 2022-04-18 from.
Schwalm, C.R., et al., 2010. Assimilation exceeds respiration sensitivity to drought: a FLUXNET synthesis. Global Change Biol. 16 (2), 657–670.
Song, L., et al., 2019. Divergent vegetation responses to extreme spring and summer droughts in Southwestern China. Agr. Forest. Meteorol. 279, 107703.
Stampfli, A., Bloor, J.M.G., Fischer, M., Zeiter, M., 2018. High land-use intensity exacerbates shifts in grassland vegetation composition after severe experimental drought. Glob. Chang Biol. 24 (5), 2021–2034.
Stuart-Haentjens, E., et al., 2018. Mean annual precipitation predicts primary production resistance and resilience to extreme drought. Sci. Total Environ. 636, 360–366.
Tian, F., Brandt, M., Liu, Y.Y., Rasmussen, K., Fensholt, R., 2017. Mapping gains and losses in woody vegetation across global tropical drylands. Glob. Chang Biol. 23 (4), 1748–1760.
Tong, X., et al., 2020. Forest management in southern China generates short term extensive carbon sequestration. Nat. Commun. 11 (1), 129.
Tong, X., et al., 2018. Increased vegetation growth and carbon stock in China karst via ecological engineering. Nat. Sustain 1 (1), 44–50.
Tong, X., et al., 2016. Assessing future vegetation trends and restoration prospects in the karst regions of Southwest China. Remote Sens. 8 (5), 357.
Tong, X., et al., 2017. Quantifying the effectiveness of ecological restoration projects on long-term vegetation dynamics in the karst regions of Southwest China. Int. J. Appl. Earth Obs. 54, 105–113.
Trugman, A.T., Anderegg, L.D.L., Shaw, J.D., Anderegg, W.R.L., 2020. Trait velocities reveal that mortality has driven widespread coordinated shifts in forest hydraulic trait composition. Proc. Natl. Acad. Sci. U. S. A. 117 (15), 8532–8538.
Wan, Z., Hook, S., Hulley, G., 2015. MOD11A1 MODIS/Terra Land Surface Temperature/Emissivity Daily L3 Global 1km SIN Grid V006 [Dataset]. NASA EOSDIS Land Processes DAAC. https://doi.org/10.5067/MODIS/MOD11A1.006. Accessed 2022-04-18 from.
Wang, H., et al., 2023. Seasonal variations in vegetation water content retrieved from microwave remote sensing over Amazon intact forests. Remote Sens. Environ. 285, 113409.
Wang, M., et al., 2021. Divergent responses of ecosystem water-use efficiency to extreme seasonal droughts in Southwest China. Sci. Total Environ. 760, 143427.
Wang, W., et al., 2010. The impact of sustained drought on vegetation ecosystem in southwest China based on remote sensing. In: Yang, Z., Chen, B. (Eds.), International Conference on Ecological Informatics and Ecosystem Conservation. Procedia Environmental Sciences, pp. 1679–1691.
Wang, Y., Xiao, J., Li, X., Niu, S., 2022. Global evidence on the asymmetric response of gross primary productivity to interannual precipitation changes. Sci. Total Environ. 814, 152786.
Wilcox, K.R., et al., 2017. Asymmetric responses of primary productivity to precipitation extremes: A synthesis of grassland precipitation manipulation experiments. Glob. Chang Biol. 23 (10), 4376–4385.
Wu, D., et al., 2018. Asymmetric responses of primary productivity to altered precipitation simulated by ecosystem models across three long-term grassland sites. Biogeosciences 15 (11), 3421–3437.
Wu, F., Deng, X., Yin, F., Yuan, Y., 2013. Projected changes of grassland productivity along the representative concentration pathways during 2010–2050 in China. Adv. Meteorol. 2013, 812723.
Yang, J., et al., 2018. Amazon drought and forest response: largely reduced forest photosynthesis but slightly increased canopy greenness during the extreme drought of 2015/2016. Glob. Chang Biol. 24 (5), 1919–1934.
Yu, G.-R., et al., 2006. Overview of ChinaFLUX and evaluation of its eddy covariance measurement. Agr. Forest. Meteorol. 137 (3-4), 125–137.
Yu, G., et al., 2016. Construction and progress of Chinese terrestrial ecosystem carbon, nitrogen and water fluxes coordinated observation. J. Geogr. Sci. 26 (7), 803–826.
Yuan, W., et al., 2016. Severe summer heatwave and drought strongly reduced carbon uptake in Southern China. Sci. Rep. 6, 18813.
Yue, Y., et al., 2022. Large scale rocky desertification reversal in South China karst. Progr. Phys. Geogr.: Earth Environ. 46 (5), 661–675.
Zeng, Y., et al., 2022. Optical vegetation indices for monitoring terrestrial ecosystems globally. Nature Rev. Earth Environ. 3 (7), 477–493.
Zhang, L., et al., 2012. The 2010 spring drought reduced primary productivity in southwestern China. Environ. Res. Lett. 7 (4), 045706.
Zhang, M., et al., 2013. Extreme drought changes in Southwest China from 1960 to 2009. J. Geogr. Sci. 23 (1), 3–16.
Zhang, X., et al., 2022. The carbon sink potential of southern China after two decades of afforestation. Earth's Future 10 (12), e2022EF002674.
Zhang, Y., et al., 2021. Author Correction: a global moderate resolution dataset of gross primary production of vegetation for 2000-2016. Sci. Data 8 (1), 67.